International Communications in Heat and Mass Transfer 63 (2015) 23–34

Contents lists available at ScienceDirect

International Communications in Heat and Mass Transfer

journal homepage: www.elsevier.com/locate/ichmt

Thermal performance of continuously moving radiative–convective fin of complex cross-section with multiple nonlinearities ☆

Ya-Song Sun [a], Jin-Liang Xu [b,*]

[a] Beijing Key Laboratory of Multiphase Flow and Heat Transfer for Low Grade Energy, North China Electric Power University, Beijing 102206, China
[b] State Key Laboratory of Alternate Electrical Power System with Renewable Energy Sources, North China Electric Power University, Beijing 102206, China

ARTICLE INFO

Available online 4 March 2015

Keywords:
Thermal performance of moving fin
Coupled radiation and convection
Complex cross-section
Variable thermal conductivity
Variable surface emissivity
Power law heat transfer coefficient

ABSTRACT

Spectral collocation method (SCM) is adopted to predict the temperature distribution in the fin with temperature dependent thermal conductivity, heat transfer coefficient and surface emissivity. These temperature dependent properties or parameters cause multiple nonlinearities of energy equation. In order to reduce these multiple nonlinearities, a local linearization approach is adopted. The spatial distribution of dimensionless temperature is discretized by Lagrange interpolation polynomials. Accordingly, the differential form of energy equation is transformed to the matrix form of algebraic equation. The accuracy of the SCM model is verified by comparing SCM results with available data in references. Meanwhile, compared with analytical solutions, it can be found that the convergence rate of SCM approximately follows exponential law. In addition, effects of various physical parameters, such as Peclet number, thermal conductivity parameter, emissivity parameter, parameter of heat transfer coefficient, convective–conductive parameter and radiative–conductive parameter on the dimensionless temperature, the dimensionless fin-tip temperature and the volume adjusted fin efficiency are comprehensively analyzed.

1. Introduction

Fined surfaces are generally used as a heat dissipation mechanism to enhance heat transfer rate between primary surface and the environment in heat exchangers [1,2]. They have widely applications in engineering industries, such as low-temperature flue gas utilization systems of waste heat energy, heat exchangers in power plants, heat exchanger of heat pump, etc. Most thermal performance analyses in the fin are based on the assumptions of uniform temperature distribution along the fin cross-section and constant thermo-physical properties. These assumptions can simplify energy equation from partial difference equation to ordinary difference equation, and the analytical solution of energy equation can be obtained. However, these assumptions are inconsistent with the thermal performances in the fin under realistic operation conditions which invariably involve multiple nonlinearities. Because of these multiple nonlinearities, it is impossible to obtain the analytical solution of energy equation. Therefore, many researchers try to solve energy equation by approximation or numerical methods.

One of nonlinearities arises when thermal conductivity is varied with temperature. If a large temperature variation exists in the fin, thermal conductivity of the fin may be varied with temperature [3]. For instance, thermal conductivity of aluminum fin decreases from 302 $W \cdot m^{-1} \cdot K^{-1}$ at 100 K to 218 $W \cdot m^{-1} \cdot K^{-1}$ at 800 K; thermal conductivity of AISI 302 stainless steel fin increases from 17.3 $W \cdot m^{-1} \cdot K^{-1}$ at 400 K to 25.5 $W \cdot m^{-1} \cdot K^{-1}$ at 1000 K [3]. As early as in the middle of 1980s, Aziz and Huq [4] gave rigorous formulations by a perturbation method, and established the optimum fin parameter on temperature dependent thermal conductivity. Coskun and Atay [5] developed the variation iteration method to analyze the fin efficiency of straight convective fins with temperature dependent thermal conductivity. Kulkarni and Joglekar [6] proposed a numerical technique based on residue minimization to solve the nonlinear energy equation in straight convective fins with temperature dependent thermal conductivity. Domairry and Fazeli [7] utilized homotopy analysis method (HAM) to evaluate the fin efficiency in the straight fin with variable thermal conductivity.

Another nonlinearity appears when heat transfer coefficient is a function of temperature. In real applications, the dependence of heat transfer coefficient is usually expressed as a power law form where its power depends on heat transfer mode like laminar natural convection, turbulent natural convection, condensation and boiling. This phenomenon had been confirmed by experimental results of Sertkaya et al. [8]. Lesnic et al. [9] presented a decomposition solution in terms of the ordinary functions of heat transfer for a straight fin. In this work, heat transfer coefficient is varied as a power–law function of the temperature difference between the surface and the convective sink. Sadri et al. [10] considered a constant cross-section area with temperature dependent thermal conductivity and heat transfer coefficient, and used differential transformation method (DTM) to obtain approximated analytical solutions for the temperature distribution and the fin efficiency. Kahani

☆ Communicated by W.J. Minkowycz.

* Corresponding author.
E-mail address: xjl@ncepu.edu.cn (J.-L. Xu).

http://dx.doi.org/10.1016/j.icheatmasstransfer.2015.01.011
0735-1933/

Nomenclature

A	thermal conductivity parameter
B	emissivity parameter
b_j	coefficient of the integral term weight
C	Fin taper ratio
C_1, C_2	constants in Eq. (36)
c_p	specific heat capacity at constant pressure, $J \cdot kg^{-1} \cdot K^{-1}$
$D_{i,j}^{(1)}$	entries of the first order derivative matrix
$D_{i,j}^{(2)}$	entries of the second order derivative matrix
$F_{i,j}$	entries of spectral coefficient matrix which are defined in Eq. (23)
$G_{i,j}$	entries of spectral coefficient matrix which are defined in Eq. (28)
H_i	entries of spectral coefficient matrix which are defined in Eq. (24)
h	convective heat transfer coefficient, $W \cdot m^{-2} \cdot K^{-1}$
h_i	barycentric Lagrange interpolation polynomials
h_L	convective heat transfer coefficient corresponding to the temperature difference $T_L - T_c$, $W \cdot m^{-2} \cdot K^{-1}$
L	fin tip length, m
l_1, l_2	adjustment parameters to reduce the nonlinearity of energy equation
m	parameter of variable heat transfer coefficient
N	total number of collocation points
N_{cc}	convective–conductive parameter
N_{rc}	radiative–conductive parameter
P	perimeter, m
Pe	Peclet number
Q_i	entries of spectral coefficient matrix which are defined in Eq. (29)
q_f	fin heat transfer rate, $W \cdot m^{-1}$
q_f^*	volume adjusted heat transfer rate, $W \cdot m^{-1}$
q_{ideal}	ideal heat transfer rate, $W \cdot m^{-1}$
R_{volume}	volume ratio
s_i	Chebyshev–Gauss–Lobatto collocation points
T	temperature, K
T_c	ambient fluid temperature, K
T_L	temperature at fin base, K
T_s	radiation sink temperature, K
w_i	entries of integral matrix defined in Eq. (31)
w_j	coefficient of Lagrange interpolation polynomials
X	dimensionless axial coordinate
x	coordinate in x-direction, m

Greek symbols

α	thermal conductivity coefficient K^{-1}
β	surface emissivity coefficient, K^{-1}
δ	semi-thickness of the fin, m
δ_0	semi-fin taper thickness, m
δ_j	parameter defined in Eq. (21)
δ_L	semi-base thickness, m
ε	surface emissivity
ε_{error}	integral averaged relative error
ε_s	surface emissivity at radiation sink temperature
η	fin efficiency
η^*	volume adjustment fin efficiency
Θ	dimensionless temperature
Θ^*	the last iterative value of dimensionless temperature
Θ_c	dimensionless environment temperature
Θ_s	dimensionless radiation sink temperature
λ	thermal conductivity, $W \cdot m^{-1} \cdot K^{-1}$
λ_0	thermal conductivity at convection sink temperature, $W \cdot m^{-1} \cdot K^{-1}$
ρ	density of the fin material, $kg \cdot m^{-3}$
σ	Stefan–Boltzmann constant, $W \cdot m^{-2} \cdot K^{-4}$

Subscripts

i,j,k	solution node indexes
max	maximum value
min	minimum value

et al. [11] utilized HAM to evaluate the analytical approximate solution and the fin efficiency of the nonlinear fin problem with variable thermal conductivity and heat transfer coefficient. Mosayebidorcheh et al. [12] used DTM to solve the nonlinear heat transfer equation of the fin when both thermal conductivity and heat transfer coefficient are power–law temperature dependent. Kani and Aziz [13] developed HAM for evaluating the thermal performance of a straight trapezoidal fin with temperature dependent thermal conductivity and heat transfer coefficient.

The other nonlinearities arise in the energy conservation equation of the fin due to the Stefan–Boltzmann law for radiation and temperature dependent internal heat generation [14]. Torabi and Aziz [15] developed DTM to analyze the thermal performance and the fin efficiency of T-shape cross-section with temperature dependent thermal conductivity, heat transfer coefficient and surface emissivity. Torabi and Zhang [16] analytically investigated the temperature distribution and efficiency of convective–radiative straight fins of various cross-sections with simultaneous variation of thermal conductivity, heat transfer coefficient, surface emissivity and internal heat generation. Recently, Torabi et al. [17] comparatively studied convective–radiative fins of rectangular, trapezoidal and concave parabolic profiles with simultaneous variation of thermal conductivity, heat transfer coefficient and surface emissivity depending on temperature.

Spectral collocation method (SCM) is a high order numerical method which is based on Chebyshev polynomials [18]. In the field of numerical simulations, lower order methods, like finite volume method and finite element method, can provide linear convergence rate, while SCM can provide exponential convergence rate [19,20]. Due to the mathematical simplicity and high accuracy with relatively few spatial grid points necessary, SCM is considered to be an efficient technique in science and engineering applications, such as computational fluid dynamics [21–23], electromagnetics [24], and magneto-hydrodynamics [25–27]. Recently, Li et al. successfully developed SCM to analyze thermal radiation heat transfer [28] and coupled radiation and conduction heat transfer [29] in the semitransparent medium.

In this research, we extend SCM to solve the radiative–convective heat transfer in the moving fin of complex cross-section with variable thermal conductivity, heat transfer coefficient, and surface emissivity. In the following, the physical model and mathematical formulations will be presented in Section 2. The accuracy and convergence rate of the SCM are demonstrated by available numerical results in the literature and analytical solutions in Section 3. In addition, effects of various parameters, including Peclet number Pe, thermal conductivity parameter A, emissivity parameter B, parameter of heat transfer coefficient m, convective–conductive parameter N_{cc}, and radiative–conductive parameter N_{rc}, on the dimensionless temperature distribution, the dimensionless fin-tip temperature and the fin efficiency in the moving fin of complex cross-section are also analyzed in Section 3. Finally, conclusions are summarized in Section 4.

2 . Physical model and mathematic formulations

2.1. Physical and mathematical models

As shown in Fig. 1, we consider the thermal processing of continuously moving fins of trapezoidal, concave parabolic and convex cross-sections with perimeter P and constant speed U. Surfaces of these

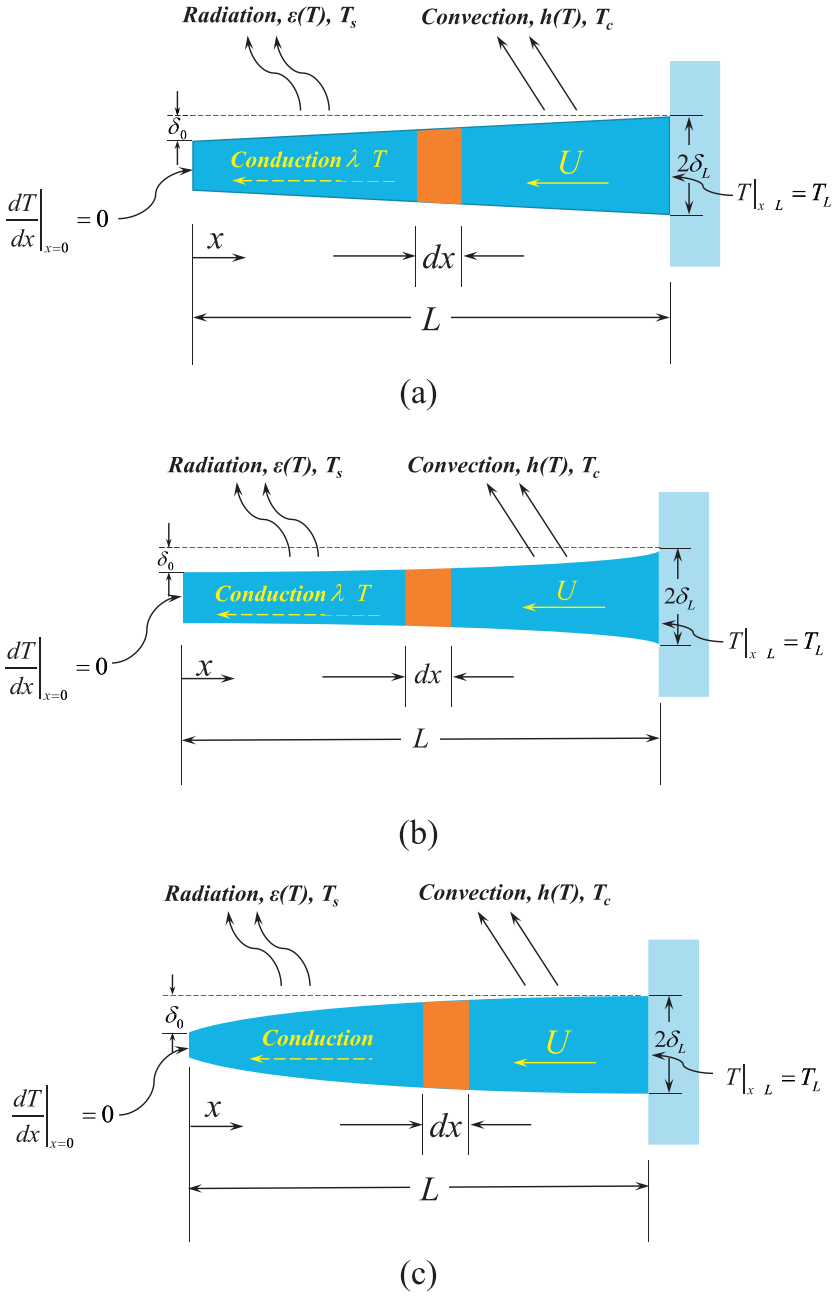

Fig. 1. Moving radiative–convective fins of different cross sections. (a) trapezoidal cross-section, (b) concave parabolic cross-section, (c) convex cross-section.

longitudinal fins transfer energy by both convection and radiation. A sink temperature $T_c < T_L$ is assumed for convective heat transfer, and other sink temperature $T_s < T_L$ is considered for radiative heat transfer. The fin tip is assumed to be adiabatic and the temperature is T_L. The radiative heat exchange between the fin and the base is neglected. If a large temperature variation exists within the fins, the thermal conductivity and the convective heat transfer coefficient of the fins may be varied with temperature, and can be taken as [10,11]

$$\lambda = \lambda_0[1 + \alpha(T - T_c)] \tag{1}$$

$$h = h_L\left(\frac{T - T_c}{T_L - T_c}\right)^m \tag{2}$$

where λ_0 is the thermal conductivity at the convective sink temperature T_c, and α is the thermal conductivity coefficient which is determined by the fin material. For example, the thermal conductivity coefficient of aluminum is $\alpha = -3.9375 \times 10^{-4}\mathrm{K}^{-1}$ when the fin temperature decreases from 800 K to 100 K [3]. h_L is the convection heat transfer coefficient corresponding to the temperature difference $T_L - T_c$; m is the parameter for variable heat transfer coefficient. For instance, $m = -1/4$, $m = 1/4$ and $m = 1/3$ for laminar film boiling or condensation, laminar natural convection, and turbulent natural convection, respectively [12].

Moreover, the surface emissivity is assumed to be the function of temperature [15]

$$\varepsilon = \varepsilon_s[1 + \beta(T - T_s)] \tag{3}$$

where ε_s is the surface emissivity at the radiation sink temperature T_s, and β is the surface emissivity coefficient.

Table 1
The local semi-fin thickness for fin of variable cross-section.

Variable cross section	The local semi-fin thickness
Trapezoidal cross section	$\delta(x)=\delta_0[(x/L)-1]+\delta_L$
Concave parabolic cross section	$\delta(x)=\delta_0[(x/L)^2-1]+\delta_L$
Convex cross section	$\delta(x)=\delta_0(x/L)^{1/2}+(\delta_L-\delta_0)$

From the view of energy conservation, the steady-stated energy equation of longitudinal fin element can be expressed as

$$\frac{d}{dx}\left[\lambda(T)\delta(x)\frac{dT}{dx}\right]-h(T)(T-T_c)-\varepsilon(T)\sigma\left(T^4-T_s^4\right)+\rho c_p\delta(x)U\frac{dT}{dx}=0 \quad (4)$$

where $\delta(x)$ is the local semi-fin thickness within the fin element, and its detailed expression is listed in Table 1. In Table 1, δ_L is the semi-base thickness; and δ_0 is the semi-fin taper thickness (see Fig. 1).

There are different types of boundary conditions for the radiative–convective moving fin, such as prescribed temperature (Dirichlet boundary condition), and prescribed heat flux (Neumann boundary condition). In the fin base boundary, the boundary condition for Eq. (4) is assumed to constant temperature

$$T(x=L)=T_L. \quad (5)$$

In the fin tip boundary, the boundary condition for Eq. (4) is assumed to adiabatic boundary

$$\left.\frac{dT}{dx}\right|_{x=0}=0. \quad (6)$$

For convenience of analysis, the energy equation and the corresponding conditions are non-dimensionalized

$$\begin{aligned}&\frac{d}{dX}\left\{[1+A(\Theta-\Theta_c)]\frac{\delta(X)}{\delta_L}\frac{d\Theta}{dX}\right\}-N_{cc}(\Theta-\Theta_c)^{m+1}\\&\quad-N_{rc}[1+B(\Theta-\Theta_s)]\left(\Theta^4-\Theta_s^4\right)+Pe\frac{\delta(X)}{\delta_L}\frac{d\Theta}{dX}=0\end{aligned} \quad (7)$$

$$\Theta(X=1)=1 \quad (8)$$

$$\left.\frac{d\Theta}{dX}\right|_{X=0}=0 \quad (9)$$

where dimensionless parameters are listed in Table 2.

Table 2
Dimensionless parameters for heat transfer in the moving radiative–convective fin.

Dimensionless parameters	Definition
Dimensionless temperature	$\Theta=\frac{T}{T_L}$
Dimensionless convective sink temperature	$\Theta_c=\frac{T_c}{T_L}$
Dimensionless radiative sink temperature	$\Theta_s=\frac{T_s}{T_L}$
Dimensionless axial coordinate	$X=\frac{x}{L}$
Convective–conductive parameter	$N_{cc}=\frac{h_L L^2 T_L^m}{\lambda_0\delta_L(T_L-T_c)^m}$,
Radiative–conductive parameter	$N_{rc}=\frac{\sigma\varepsilon_s L^2 T_L^3}{\lambda_0\delta_L}$
Thermal conductivity parameter	$A=\alpha T_L$
Emissivity parameter	$B=\beta T_L$
Fin taper ratio	$C=\frac{\delta_0}{\delta_L}$
Peclet number	$Pe=\frac{LU\rho c_p}{\lambda_0}$

Eq. (7) has multiple nonlinearities due to temperature dependent thermal conductivity, heat transfer coefficient and surface emissivity. To reduce these nonlinearities, Eq. (7) can be rewritten as

$$\begin{aligned}&[1+A(\Theta-\Theta_c)]\frac{\delta(X)}{\delta_L}\frac{d^2\Theta}{dX^2}+[1+A(\Theta-\Theta_c)]\left[\frac{1}{\delta_L}\frac{d\delta(X)}{dX}\right]\frac{d\Theta}{dX}\\&+Pe\frac{\delta(X)}{\delta_L}\frac{d\Theta}{dX}+l_1N_{cc}\Theta^{m+1}+l_2N_{rc}[1+B(\Theta-\Theta_s)]\Theta^4\\&=N_{cc}(\Theta-\Theta_c)^{m+1}+N_{rc}[1+B(\Theta-\Theta_s)]\left(\Theta^4-\Theta_s^4\right)\\&-A\frac{\delta(X)}{\delta_L}\left(\frac{d\Theta}{dX}\right)^2+l_1N_{cc}\Theta^{m+1}+l_2N_{rc}[1+B(\Theta-\Theta_s)]\Theta^4\end{aligned} \quad (10)$$

where l_1 and l_2 are adjustment parameters, and these values of l_1 and l_2 are subjected to convection–conduction parameter and radiation–conduction parameter.

The fin heat transfer rate q_f can be computed by integrating the convective and radiative heat losses from the surface of the fin as follows

$$q_f=\int_0^L\left\{h_LP(x)\frac{(T-T_c)^{m+1}}{(T_L-T_c)^m}+P(x)\sigma\varepsilon_s[1+\beta(T-T_s)]\left(T^4-T_s^4\right)\right\}dx. \quad (11)$$

The ideal fin heat transfer rate q_{ideal} is realized if the entire fin is maintained at the base temperature, and may be found as

$$q_{ideal}=\int_0^L\left\{LP(x)h_L\frac{(T_b-T_c)^{m+1}}{(T_L-T_c)^m}+LP(x)\sigma\varepsilon_s[1+\beta(T-T_s)]\left(T^4-T_s^4\right)\right\}dx. \quad (12)$$

The fin efficiency η is defined as the ratio of the fin heat transfer rate q_f and the ideal fin heat transfer rate q_{ideal} as follows [15]

$$\eta=\frac{q_f}{q_{ideal}}=\frac{\int_0^1\left[N_{cc}(\Theta-\Theta_c)^{m+1}+N_{rc}[1+B(\Theta-\Theta_s)]\left(\Theta^4-\Theta_s^4\right)\right]dX}{N_{cc}(1-\Theta_c)^{m+1}+N_{rc}[1+B(1-\Theta_s)](1-\Theta_s^4)}. \quad (13)$$

However, for the comparison of the fin efficiency for trapezoidal and concave parabolic cross-sections, the difference in the amount of material for these fins should be taken into account. The ratio of volume R_{volume} for different cross-sections can be computed as

$$\begin{aligned}R_{volume}&=\frac{V_t\text{ or }V_c}{V_r}=\frac{\int_0^L\{\delta_L+\delta_0[(x/L)^n-1]\}dx}{L\delta_L}\\&=\int_0^1[1+C(X^n-1)]dX=1-\frac{Cn}{n+1}.\end{aligned} \quad (14)$$

Hence, the volume adjusted heat transfer rate q_f^* can be obtained by the fin heat transfer rate q_f to divide the volume ratio R_{volume}. The volume adjusted fin efficiency is expressed as

$$\eta^*=\frac{q_f^*}{q_{ideal}}=\frac{q_f}{R_{volume}q_{ideal}}=\frac{\eta}{R_{volume}}. \quad (15)$$

2.2. Spectral collocation method formulation

For the dimensionless energy equation, the non-periodic spatial domain is discretized by the Chebyshev–Gauss–Lobatto (CGL) collocation points [20]

$$s_i=-\cos\left[\frac{\pi(i-1)}{N-1}\right],\quad i=1,2,\cdots,N \quad (16)$$

where N is the total number of collocation points.

In order to fit the requirement of Chebyshev polynomials, the following transformation should be used to map arbitrary interval $[X_{\min}, X_{\max}]$ into standard interval $[-1,1]$

$$X = \frac{1}{2}[(X_{\max}-X_{\min})s + ((X_{\max}+X_{\min}))]. \tag{17}$$

After mapping, Eq. (10) can be written as

$$\begin{aligned}
&[1+A(\Theta-\Theta_c)]\frac{\delta(s)}{\delta_L}\left(\frac{X_{\max}-X_{\min}}{2}\right)^2\frac{d^2\Theta}{ds^2}\\
&+[1+A(\Theta-\Theta_c)]\left[\frac{1}{\delta_L}\frac{d\delta(s)}{ds}\right]\left(\frac{X_{\max}-X_{\min}}{2}\right)^2\frac{d\Theta}{ds}\\
&+Pe\frac{\delta(s)}{\delta_L}\left(\frac{X_{\max}-X_{\min}}{2}\right)\frac{d\Theta}{ds}+l_1N_{cc}\Theta^{m+1}+l_2N_{rc}[1+B(\Theta-\Theta_s)]\Theta^4\\
&=N_{cc}(\Theta-\Theta_c)^{m+1}+N_{rc}[1+B(\Theta-\Theta_s)]\left(\Theta^4-\Theta_s^4\right)\\
&-A\frac{\delta(s)}{\delta_L}\left(\frac{X_{\max}-X_{\min}}{2}\right)^2\left(\frac{d\Theta}{ds}\right)^2+l_1N_{cc}\Theta^{m+1}+l_2N_{rc}[1+B(\Theta-\Theta_s)]\Theta^4.
\end{aligned} \tag{18}$$

The dimensionless temperature can be approximated by Lagrange interpolation polynomials, like

$$\Theta(s)\approx\sum_{i=1}^{N}\Theta(s_i)h_i(s) \tag{19}$$

where $h_i(s)$ are functions of the barycentric Lagrange interpolation polynomials [19]

$$h_i(s)=\frac{w_i'/(s-s_i)}{\sum_{j=1}^{N}w_j'/\left(s-s_j\right)} \tag{20}$$

where

$$w_j'=(-1)^{j-1}\delta_j',\quad \delta_j'=\begin{cases}1/2, & j=1,N\\ 1, & \text{otherwise}\end{cases}. \tag{21}$$

Substituting the approximation of dimensionless temperature (Eq. (19)) into the dimensionless energy equation (Eq. (18)), one can obtain the matrix form of spectral discretized algebraic equation

$$\begin{bmatrix}F_{1,1}&F_{1,2}&\cdots&F_{1,N}\\F_{2,1}&F_{2,2}&\cdots&F_{2,N}\\\vdots&\vdots&\ddots&\vdots\\F_{N,1}&F_{N,2}&\cdots&F_{N,N}\end{bmatrix}\begin{bmatrix}\Theta_1\\\Theta_2\\\vdots\\\Theta_N\end{bmatrix}=\begin{bmatrix}H_1\\H_2\\\vdots\\H_N\end{bmatrix} \tag{22}$$

where the elements of matrices $F_{i,j}$ and H_i are defined as

$$F_{i,j}=\begin{cases}
\begin{aligned}&[1+A(\Theta_i^*-\Theta_c)]\left(\frac{X_{\max}-X_{\min}}{2}\right)^2\frac{\delta_i}{\delta_L}D_{i,j}^{(2)}\\&+[1+A(\Theta_i^*-\Theta_c)]\left(\frac{X_{\max}-X_{\min}}{2}\right)^2\left(\sum_{k=1}^{N}D_{i,k}^{(1)}\delta_k\right)D_{i,j}^{(1)}\\&+Pe\left(\frac{X_{\max}-X_{\min}}{2}\right)\frac{\delta_i}{\delta_L}D_{i,j}^{(1)}+l_1N_{cc}(\Theta_i^*)^m\\&+l_2N_{rc}[1+B(\Theta_i^*-\Theta_s)](\Theta_i^*)^3\end{aligned} & i=j\\
\begin{aligned}&[1+A(\Theta_i^*-\Theta_c)]\left(\frac{X_{\max}-X_{\min}}{2}\right)^2\frac{\delta_i}{\delta_L}D_{i,j}^{(2)}\\&+[1+A(\Theta_i^*-\Theta_c)]\left(\frac{X_{\max}-X_{\min}}{2}\right)^2\left(\sum_{k=1}^{N}D_{i,k}^{(1)}\delta_k\right)D_{i,j}^{(1)}\\&+Pe\left(\frac{X_{\max}-X_{\min}}{2}\right)\frac{\delta_i}{\delta_L}D_{i,j}^{(1)}\end{aligned} & i\neq j
\end{cases} \tag{23}$$

$$\begin{aligned}
H_i=&N_{cc}(\Theta_i^*-\Theta_c)^{m+1}+N_{rc}[1+B(\Theta_i^*-\Theta_s)]\left[(\Theta_i^*)^4-\Theta_s^4\right]\\
&-A\frac{\delta_i}{\delta_L}\left(\frac{X_{\max}-X_{\min}}{2}\right)^2\left(\sum_{k=1}^{N}D_{i,k}^{(1)}\Theta_k^*\right)^2\\
&+l_1N_{cc}(\Theta_i^*)^{m+1}+l_2N_{rc}[1+B(\Theta_i^*-\Theta_s)](\Theta_i^*)^4
\end{aligned} \tag{24}$$

where Θ^* denotes the last iterative value of dimensionless temperature, $D_{i,j}^{(1)}$ and $D_{i,j}^{(2)}$ are entries of the first order and the second order derivative coefficient matrices, respectively [18].

Similarly, the spectral discretization of Neumann boundary condition (Eq. (9)) can be written as

$$\begin{bmatrix}D_{1,1}^{(1)}&D_{1,2}^{(1)}&\cdots&D_{1,N}^{(1)}\end{bmatrix}\begin{bmatrix}\Theta_1\\\Theta_2\\\vdots\\\Theta_N\end{bmatrix}=0. \tag{25}$$

Importing Dirichlet and Neumann boundary conditions, the spectral discretization of energy equation can be rewritten in the matrix form as follows.

$$\begin{bmatrix}D_{1,1}&D_{1,2}&\cdots&D_{1,N-1}&D_{1,N}\\F_{2,1}&F_{2,2}&\cdots&F_{2,N-1}&F_{2,N}\\\vdots&\vdots&\ddots&\vdots&\vdots\\F_{N-1,1}&F_{N-1,2}&\cdots&F_{N-1,N-1}&F_{N-1,N}\\F_{N,1}&F_{N,2}&\cdots&F_{N,N-1}&F_{N,N}\end{bmatrix}\begin{bmatrix}\Theta_1\\\Theta_2\\\vdots\\\Theta_{N-1}\\1\end{bmatrix}=\begin{bmatrix}0\\H_2\\\vdots\\H_{N-1}\\H_N\end{bmatrix}\begin{matrix}\leftarrow\text{known}\\\\\\\\\leftarrow\text{ignored}\end{matrix}$$
$$\text{known}\uparrow \tag{26}$$

Stripping the last row and column of the first matrix on the right hand of Eq. (26), Eq. (26) can be rearranged as the following

$$\begin{bmatrix}G_{1,1}&G_{1,2}&\cdots&G_{1,N-1}\\G_{2,1}&G_{2,2}&\cdots&G_{2,N-1}\\\vdots&\vdots&\ddots&\vdots\\G_{N-1,1}&G_{N-1,2}&\cdots&G_{N-1,N-1}\end{bmatrix}\begin{bmatrix}\Theta_1\\\Theta_2\\\vdots\\\Theta_{N-1}\end{bmatrix}=\begin{bmatrix}Q_1\\Q_2\\\vdots\\Q_{N-1}\end{bmatrix} \tag{27}$$

where

$$G_{i,j}=\begin{cases}D_{1,j}^{(1)} & i=1\\ F_{i,j} & i\neq 1\end{cases} \tag{28}$$

$$Q_i=\begin{cases}-D_{1,N} & i=1\\ H_i-F_{i,N} & i\neq 1\end{cases}. \tag{29}$$

Substituting Eq. (19) into Eq. (13), the spectral discretized form of fin efficiency can be written as

$$\begin{aligned}
\eta&=\frac{\sum_{i=1}^{N}\left\{N_{cc}(\Theta_i-\Theta_c)^{m+1}+N_{rc}[1+B(\Theta_i-\Theta_s)]\left(\Theta_i^4-\Theta_s^4\right)\right\}\int_0^1h_i(s)ds}{N_{cc}(1-\Theta_c)^{m+1}+N_{rc}[1+B(1-\Theta_s)](1-\Theta_s^4)}\\
&=\frac{\sum_{i=1}^{N}\left\{N_{cc}(\Theta_i-\Theta_c)^{m+1}+N_{rc}[1+B(\Theta_i-\Theta_s)]\left(\Theta_i^4-\Theta_s^4\right)\right\}w_i}{N_{cc}(1-\Theta_c)^{m+1}+N_{rc}[1+B(1-\Theta_s)](1-\Theta_s^4)}
\end{aligned} \tag{30}$$

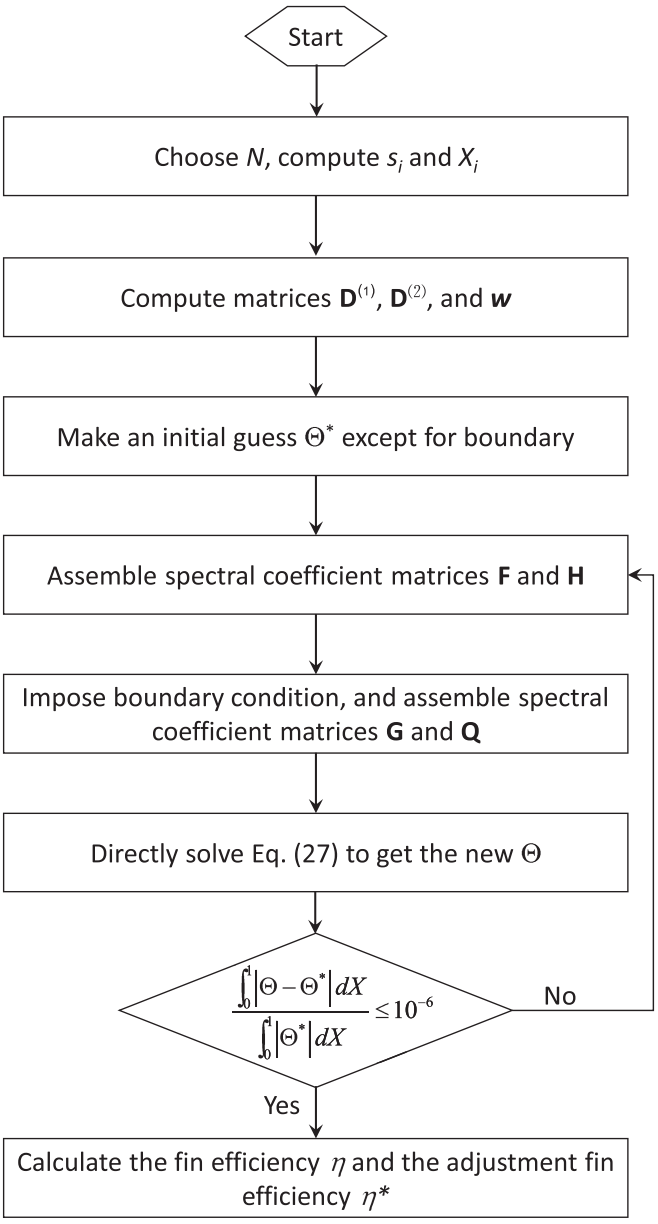

Fig. 2. The flow chart of the implementation steps.

where w_i are entries of the integral term weight corresponding to CGL collocation points, and their detailed expression are [20]

$$w_i = \frac{2}{Nc_i}\sum_{j=\text{odd}} b_j c_j \cos\left[\frac{(i-1)(j-1)\pi}{N}\right] \tag{31}$$

in which $b_j = \begin{cases} 0, & j = \text{even} \\ \frac{2}{1-(j-1)^2}, & j = \text{odd} \end{cases}$.

2.3. Solution procedures

As shown in Fig. 2, the implementation of SCM for solving nonlinear heat transfer in moving radiative–convection fin of complex cross-section can be executed through the following routine.

Step 1. Choose the number of collocation points *N*, compute CGL collocation points s_i, and then compute the coordinate values X_i by the transformation equation (Eq. (17)).

Step 2. Compute the first order derivative matrix $\mathrm{D}^{(1)}$, the second order derivative matrix $\mathrm{D}^{(2)}$, and the integral matrix w.

Step 3. Give the dimensionless temperature an initial assumption Θ^* (zero, for example) in all nodes except for boundary.

Step 4. Assemble spectral coefficient matrices *F* and *H* by Eqs. (23) and (24).

Step 5. Impose the boundary conditions, and compute spectral coefficient matrices *G* and *Q* by Eqs. (28) and (29).

Step 6. Directly solve the matrix Eq. (27) to get the new dimensionless temperature Θ.

Step 7. If the convergence criteria (Eq. (32)) is satisfied, terminate the iteration and go to step 8. Otherwise, renew the dimensionless temperature and go back to step 4.

Step 8. Compute the fin efficiency and the adjustment fin efficiency by Eqs. (30) and (15).

The convergence criteria of dimensionless temperature is

$$\frac{\int_0^1 |\Theta-\Theta^*|dX}{\int_0^1 |\Theta^*|dX} \le 10^{-6}. \tag{32}$$

3 . Results and discussions

Compared with FVM, FDM and FEM, the main superiorities of SCM are exponential convergence and high accuracy [18]. In this paper, we analyze the performance characteristics of moving radiative–convective fins of trapezoidal, concave parabolic and convex cross-sections with temperature dependent of thermal conductivity, heat transfer coefficient and surface emissivity. For convenience, Results and discussions are divided into five sub-sections. Firstly, the SCM results are checked against benchmark solutions which are solved by DTM. These comparisons are adopted in order to verify the accuracy of SCM. Secondly, the effect of number of collocation points on dimensionless temperature is analyzed, and the convergence characteristic of the SCM for the moving radiative–convective fin is examined. Thirdly, some figures are illustrated about the effects of physical parameters such as Peclet number *Pe*, thermal conductivity parameter *A*, emissivity parameter *B*, parameter of heat transfer coefficient *m*, convective–conductive parameter N_{cc}, and radiative–conductive parameter N_{rc} on dimensionless temperature distributions within the moving fin. Finally, some figures are illustrated about effects of aforementioned parameters on the dimensionless fin-tip temperature. Fourthly, some figures are also shown about effects of aforementioned parameters on the fin-tip temperature in the moving fin. Finally, effects of aforementioned parameters on the fin efficiency of the moving fin are analyzed. All computations of SCM formulations are carried out on a computer with Inter Core I5 2.40 GHz processor and 2.0 GB RAM memory.

3.1. Validation of model

In order to validate above SCM formulations, we consider stationary radiative–convective fins of trapezoidal, concave parabolic and convex cross-sections with variable thermal conductivity, heat transfer coefficient and surface emissivity.

For the sake of quantitative comparison SCM results and available data in the literature, the integral averaged relative error is defined as

$$\varepsilon_{\text{error}} = \frac{\int |R_{\text{SCM}}(x) - R_{\text{Benchmark}}(x)|dx}{\int R_{\text{benchmark}}(x)dx} \tag{33}$$

where R_{SCM} is the SCM solution, $R_{\text{Benchmark}}$ is the Benchmark solution.

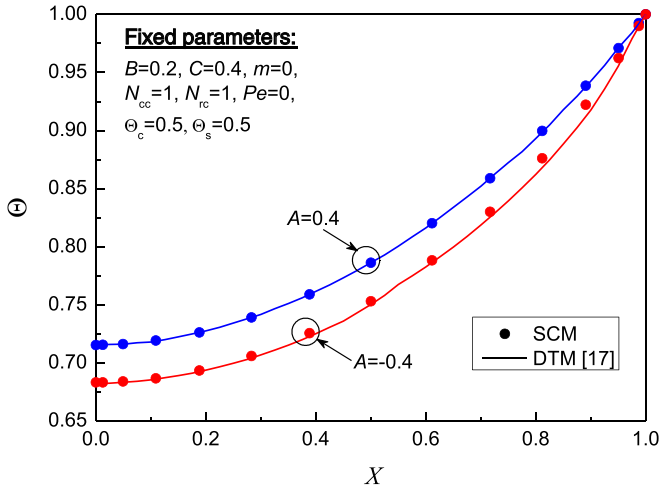

Fig. 3. Comparison of the SCM results with the analytical solutions for (a) trapezoidal cross-section, (b) concave parabolic cross-section, (c) convex cross-section.

The dimensionless temperature distributions by SCM within the trapezoidal fin are shown in Fig. 3(a) for two different thermal conductivity parameters, namely, $A = 0.4$ and $A = -0.4$. In the trapezoidal fin, the surface emissivity is a linear function of temperature as $\varepsilon(T) = \varepsilon_s[1 + 0.2(\Theta - \Theta_s)]$, and the convective heat transfer is $h = h_L$. Convective–conductive parameter is $N_{cc} = 1$, radiative–conductive parameter is $N_{rc} = 1$, the convective sink temperature is $\Theta_c = 0.5$ and the radiative sink temperature $\Theta_s = 0.5$. As shown in Fig. 3(a), the results of present method in this paper are in good agreement with those of DTM [17] for different thermal conductivity parameters. Compared with the results of DTM [17], the integral averaged relative errors are 0.14% and 0.43% at thermal conductive parameters $A = 0.4$ and $A = -0.4$, respectively.

Next, we consider a concave parabolic fin with different convective heat transfer modes, where $m = 0$ and $m = 2$ are for forced convection and nucleate boiling, respectively. The thermal conductivity and the surface emissivity of the concave parabolic fin vary linearly with temperature and can be expressed as $\lambda(T) = \lambda_0[1 + 0.4(\Theta - \Theta_c)]$ and $\varepsilon(T) = \varepsilon_s[1 + 0.2(\Theta - \Theta_s)]$, respectively. Other physical parameters are the same as above. The dimensionless temperature distributions of SCM are shown in Fig. 3(b) for different parameters of heat transfer coefficient. There is no observable difference between the results of SCM and DTM [17].

In order to further prove the accuracy of SCM, more comparisons between the results of SCM and those available results in Ref. [16] are made. In Fig. 3(c), the dimensionless temperature distributions in convex fin are shown for different convective–conductive parameters with $N_{cc} = 0.5$ and $N_{cc} = 1.0$. The remaining parameters are $A = 0.2$, $B = 0.2$, $C = 1.0$, $N_{rc} = 1.0$, $Pe = 0.0$, $\Theta_c = 0.5$ and $\Theta_s = 0.5$. This case was also studied by Torabi and Zhang using the DTM [16]. As shown in Fig. 3(c), it is seen that results of SCM match very well with those of DTM [16]. The integral relative errors between SCM and DTM are 0.19% and 0.18% for $N_{cc} = 0.1$ and $N_{cc} = 1.0$, respectively.

3.2. Effect of the number of collocation points

In order to analyze the effect of the number of collocation points, we consider moving radiative–convective fin of rectangular cross section with a constant thermal conductivity ($A = 0$), a constant heat transfer coefficient ($m = 0$) and pure convection ($N_{rc} = 0$). The governing equation is reduced to

$$\frac{d^2\Theta}{dX^2} - N_{cc}(\Theta - \Theta_c) + Pe\frac{d\Theta}{dX} = 0 \tag{34}$$

with boundary conditions (Eqs. (8) and (9)).

Then, the analytic solution of Eq. (35) can be derived as

$$\Theta(X) = C_1 e^{-\left(\frac{Pe+\sqrt{Pe^2+4N_{cc}}}{2}X\right)} + C_2 e^{-\left(\frac{Pe-\sqrt{Pe^2+4N_{cc}}}{2}X\right)} + \Theta_c \tag{35}$$

where constants are same as follows

$$C_1 = C_2 = \frac{\left(Pe+\sqrt{Pe^2+4N_{cc}}\right)(\Theta_c - 1)}{\left(Pe-\sqrt{Pe^2+4N_{cc}}\right)e^{-\left(\frac{Pe+\sqrt{Pe^2+4N_{cc}}}{2}\right)} - \left(Pe+\sqrt{Pe^2+4N_{cc}}\right)e^{-\left(\frac{Pe-\sqrt{Pe^2+4N_{cc}}}{2}\right)}}. \tag{36}$$

Fig. 4(a) shows the effect of the number of collocation points on dimensionless distributions in the radiative–convective fin for three values of convection–conduction parameters, namely, $N_{cc} = 0.5$, 1 and 5. In this case, the Peclet number is $Pe = 0$, and the convective sink temperature is $\Theta_c = 0.5$. For the case of $N_{cc} = 0.5$, the integral averaged relative errors between SCM results and analytical solutions are 2.32×10^{-4}, 7.01×10^{-8} and 2.53×10^{-10} for $N = 7$, $N = 11$ and $N = 15$, respectively. There are no significant differences between SCM results with $N = 15$ and analytical solution.

Moreover, for the sake of quantitative analyzing the effect of the total number of collocation points, the integral relative errors between

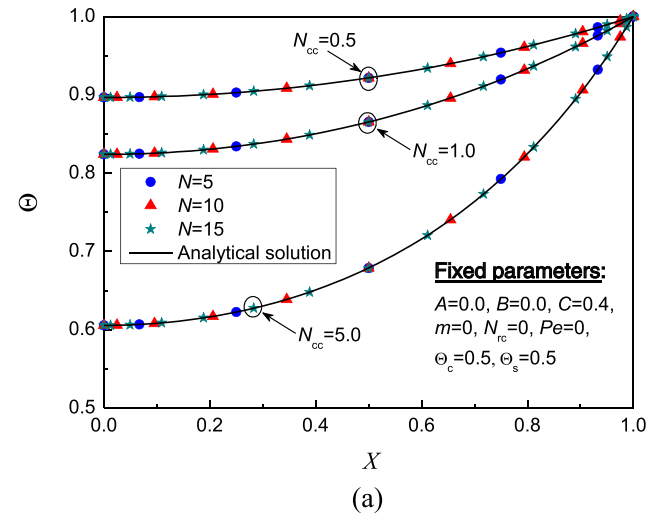

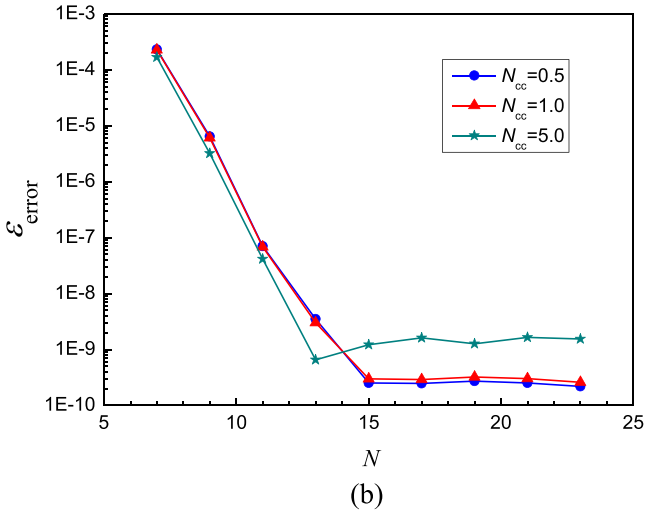

Fig. 4. Effect of the number of collocation points on (a) dimensionless temperature distribution, (b) integral averaged relative error.

SCM results and analytical solutions are given in Fig. 4(b). It can be seen that the convergence rate of the SCM is very fast and approximately follows an exponential law trend. As shown in Fig. 4(b), the integral relative error is less than 1.2195×10^{-9} for $N = 15$. The integral averaged relative error does not obviously decrease when the total number of collocation points is greater than $N = 15$. A similar trend is also discovered for other parameters. Therefore, $N = 15$ is used for spatial discretization in the following simulations.

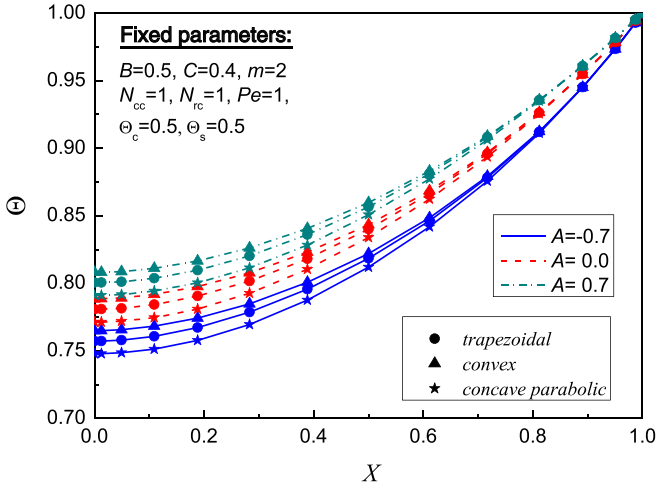

Fig. 6. Effect of *A* for dimensionless temperature distributions with different cross-sections.

3.3. Distribution of dimensionless temperature

Fig. 5 illustrates the effect of Peclet number on the distributions of dimensionless temperature along the moving radiative–convective fins of trapezoidal, convex and concave parabolic cross-sections. It is evident that the dimensionless temperature distribution generally increases with the increasing of Peclet number. The Peclet number is the ratio of thermal adventive transport rate to thermal diffusive transport rate in the moving fin. When the Peclet number increases, the fin moves faster and the exposure time to the surroundings gets shorter. Hence, the dimensionless temperature becomes higher. Otherwise, Fig. 5 also shows that the dimensionless temperature distribution is greatly dependent on the shape of cross-section. The dimensionless temperature gets higher for the convex fin, while the dimensionless temperature gets lower for the concave parabolic fin.

Fig. 6 shows the dimensionless temperatures in trapezoidal, convex and concave parabolic fins for different thermal conductivity parameters, namely, $A = -0.7$, 0.0 and 0.7. For this case, the fixed parameters

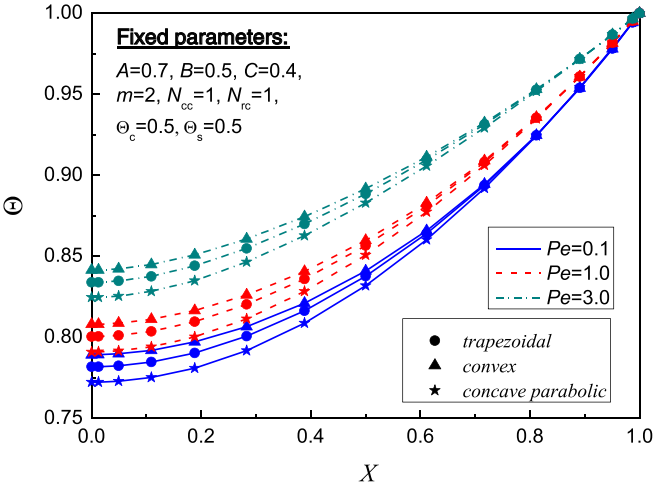

Fig. 5. Effect of *Pe* for dimensionless temperature distributions with different cross-sections.

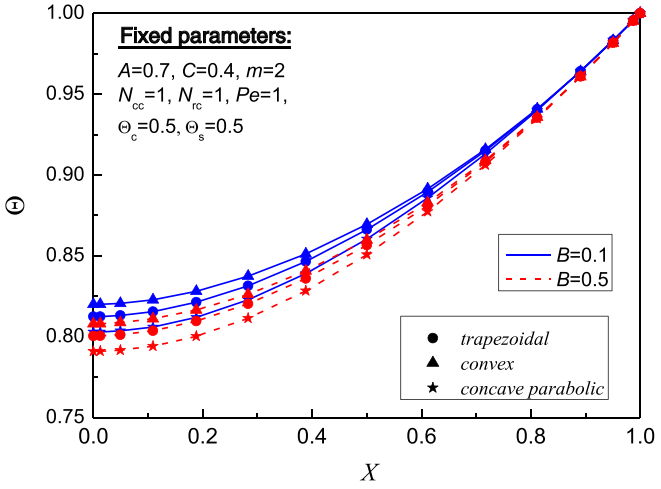

Fig. 7. Effect of *B* for dimensionless temperature distributions with different cross-sections.

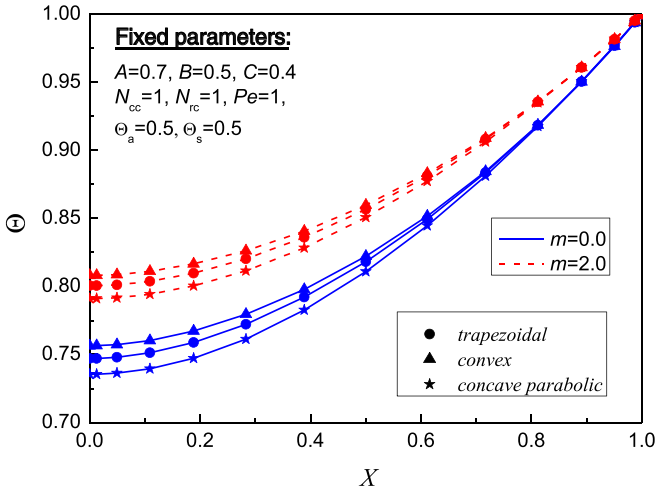

Fig. 8. Effect of m for dimensionless temperature distributions with different cross-sections.

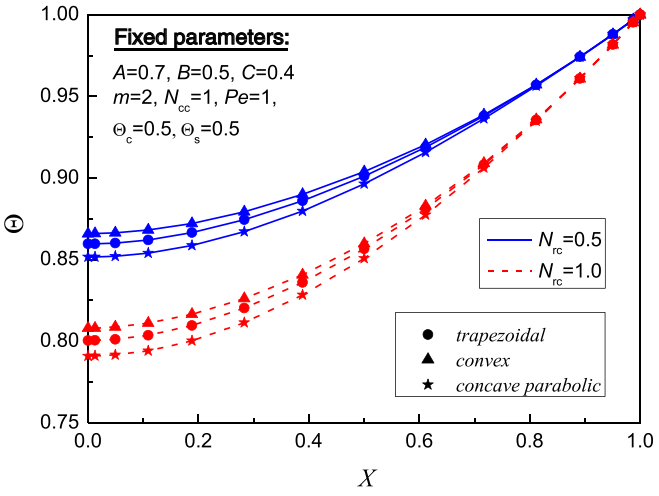

Fig. 10. Effect of N_{rc} for dimensionless temperature distributions with different cross-sections.

are $B = 0.5$, $C = 0.4$, $m = 2$, $N_{cc} = 1.0$, $N_{rc} = 1.0$, $Pe = 1.0$, $\Theta_c = 0.5$ and $\Theta_s = 0.5$. It can be seen that the dimensionless temperature gradually increases with the increasing of thermal conductivity coefficient. This trend becomes more obvious in the fin tip. The reason can be explained that for $A = 0.7$, the thermal conductivity in the fin is proportional to the dimensionless temperature, and conduction heat transfer in the fin is enhanced. For $A = -0.7$, the phenomenon is just on the contrary.

In Fig. 7, effect of surface emissivity parameter B has been shown on the dimensionless temperature distribution in the moving fin of complex cross-section. It is seen from Fig. 7 that the dimensionless temperature in the fin increases with increasing surface emissivity parameter. As surface emissivity parameter increases from $B = 0.1$ to $B = 0.5$, the average surface emissivity increases, and this leads to more radiative heat loss from the fin surface. In addition, the effect of surface emissivity parameter on the dimensionless temperature is maximum for the concave parabolic fin; while it is minimum for the convex fin.

Fig. 8 shows the dimensionless temperature in the fin with constant and variable heat transfer coefficients for assessing the effect of parameter of heat transfer coefficient m. The curves marked with $m = 0$ are corresponding to the temperature distribution with constant heat transfer coefficient $h = h_L$; while the curves marked with $m = 2$ imply the temperature distribution with nucleate boiling heat transfer $h = h_L\left(\frac{T-T_c}{T_L-T_c}\right)^2$. Compared with constant heat transfer coefficient ($m = 0$), variable heat transfer coefficient ($m = 2$) can produce the higher dimensionless temperature. Because the average convective heat transfer coefficient with $m = 2$ is less than heat transfer coefficient at the fin base temperature h_L, then this will result in the reducing of convection heat loss. Otherwise, Fig. 7 also shows that the effect of variable heat transfer coefficient on the dimensionless temperature distribution is greatly dependent on the shape of cross-section. The deviation of the dimensionless temperature for different parameters of heat transfer coefficient increases from trapezoidal cross-section to convex cross-section, then to concave parabolic cross-section.

In Figs. 9 and 10, effects of convective–conductive parameter N_{cc} and radiative–conductive parameter N_{rc} on the dimensionless temperature distribution have been given for $A = 0.7$, $B = 0.5$, $C = 0.4$, $m = 2$, $Pe = 1.0$, $\Theta_c = 0.5$ and $\Theta_s = 0.5$. We can see from Figs. 9 and 10 that for a constant N_{rc}, variable N_{cc} is imposing significant effect on the dimensionless temperature distribution, and for a given N_{cc}, N_{rc} is also exerting a major effect on the dimensionless temperature distribution. N_{cc} is defined to be the ratio of convection heat loss from the fin surface to conduction heat transfer in the fin. Similarly, N_{rc} is defined as the ratio of radiation heat loss from the fin surface to conduction heat transfer in the fin. As the N_{cc} increases, it leads to more heat loss from the fin surface. Hence, the dimensionless temperature distribution becomes steeper from left to right. Fig. 10 also demonstrates that N_{rc} has a

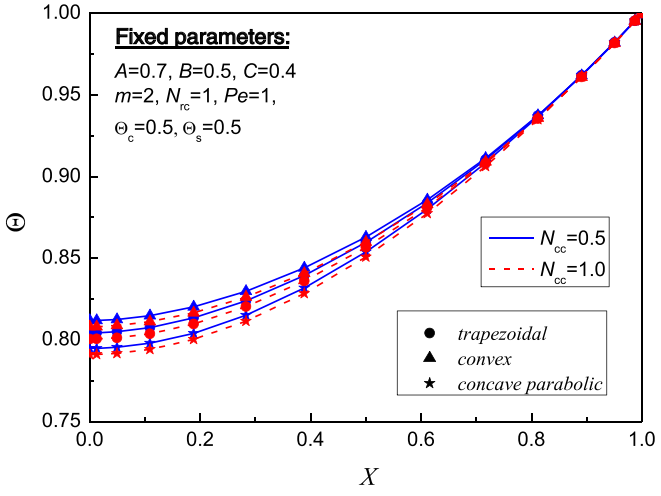

Fig. 9. Effect of N_{cc} for dimensionless temperature distributions with different cross-sections.

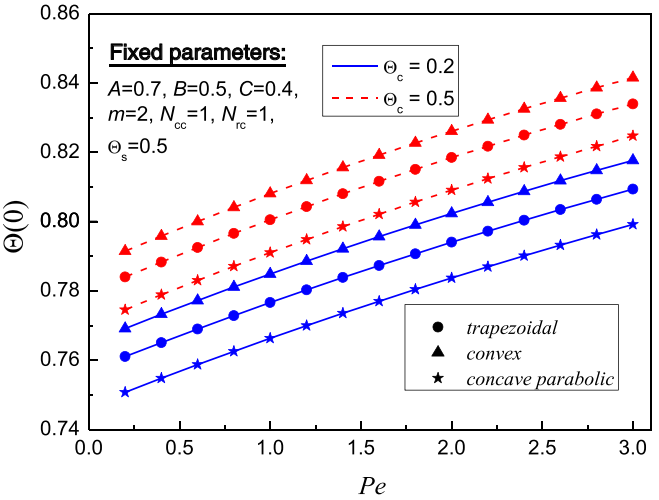

Fig. 11. Effect of Pe and Θ_c on the dimensionless fin tip temperature.

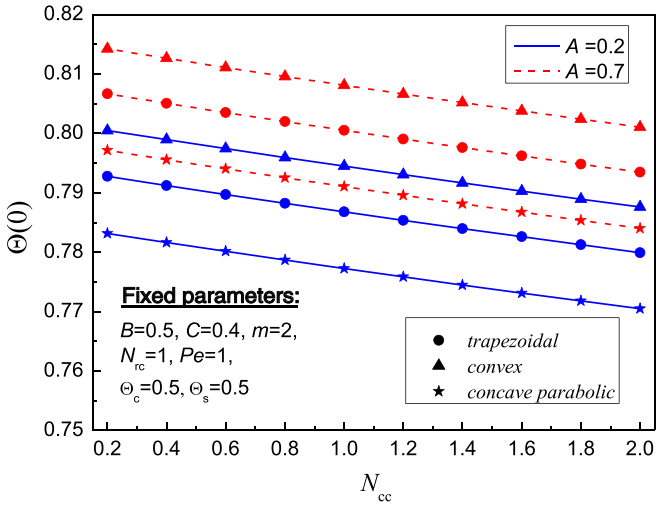

Fig. 12. Effect of N_{cc} and A on the dimensionless fin tip temperature.

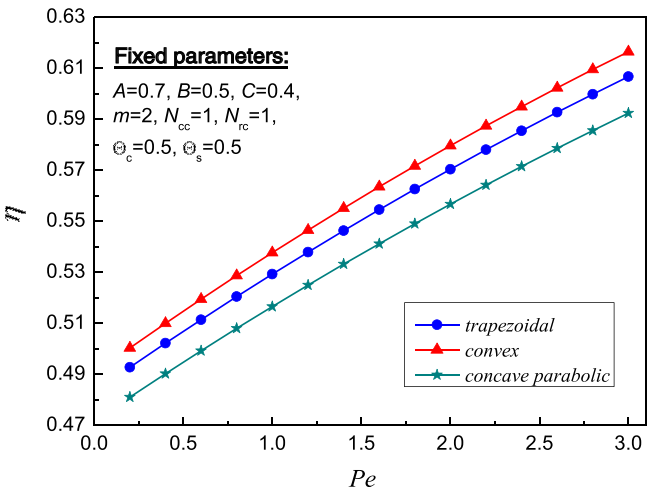

Fig. 14. Effect of Pe on fin efficiency for different cross-sections.

minimum effect on the dimensionless temperature for the trapezoidal fin, while it shows a maximum effect for the concave parabolic fin. Furthermore, comparing Figs. 9 and 10, one can see that N_{rc} imposes more obvious effect on the dimensionless temperature distribution than N_{cc} does.

3.4. Dimensionless fin-tip temperature

The dimensionless fin-tip temperature in the moving fin of complex cross-section varying with the Peclet number under different convective sink temperature $\Theta_c = 0.2$ and 0.5, is depicted in Fig. 11. The other dimensionless parameters are $A = 0.7$, $B = 0.5$, $C = 0.4$, $m = 2$, $N_{cc} = 1.0$, $N_{rc} = 1.0$, $\Theta_c = 0.4$ and $\Theta_s = 0.5$. As demonstrated in Fig. 11, the dimensionless fin-tip temperature increases as the Peclet number and convective sink temperature increase. Otherwise, the convex fin gives higher dimensionless fin-tip temperature compared with that of trapezoidal and concave parabolic fins.

In Fig. 12, we have analyzed the effect of convective–conductive parameter and thermal conductivity parameter on the dimensionless fin-tip temperatures for various cross-sections. The dimensionless fin-tip temperature decreases with the increasing of the convective–conductive parameter. The reason is that as convective–radiative parameter increases, convective heat transfer along the moving fin is stronger, and it attributes to more heat loss from the moving fin. Moreover, as the thermal conductivity parameter increases for the fixed convective–conductive parameter, the dimensionless fin-tip temperature increases. The reason can be explained that conductive heat transfer is enhanced as the dimensionless thermal conductivity coefficient of the moving fin increases, and results in the increasing of dimensionless fin-tip temperature.

Similarly, the same variation trend of the dimensionless fin-tip temperature, radiative–conductive parameter and the parameter of heat transfer coefficient is drawn in Fig. 13. The increasing of the radiative–conductive parameter means enhancement of radiative heat transfer. It attributes to more heat loss from the moving fin by radiation, and decreases the dimensionless fin-tip temperature. Moreover, the average convective heat transfer coefficient with $m = 2$ is less than constant heat transfer coefficient with $m = 0$. It attributes to loss convective heat loss from the fin of various cross-section, and results in the higher dimensionless fin-tip temperature.

3.5. Fin efficiency

Fig. 14 presents the effect of the Peclet number on the fin efficiency for trapezoidal, convex and concave parabolic fins. The fin efficiency increases as the Peclet number increases. The reason is that, as the Peclet number increases, the speed of the moving fin becomes faster and the exposure time to the surroundings gets shorter. The dimensionless

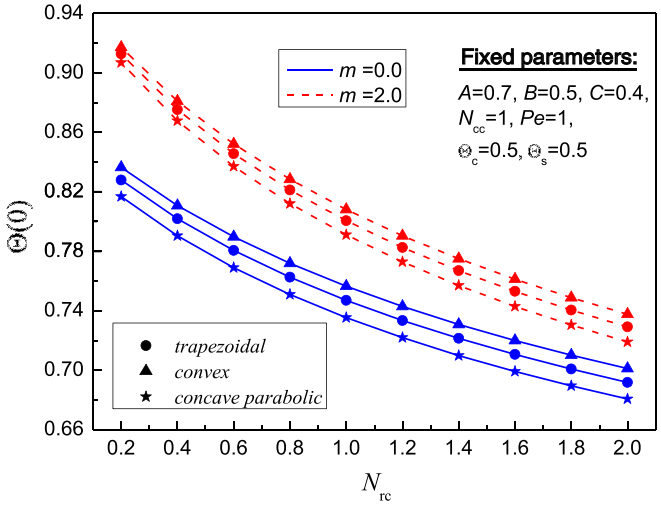

Fig. 13. Effect of N_{rc} and m on the dimensionless fin tip temperature.

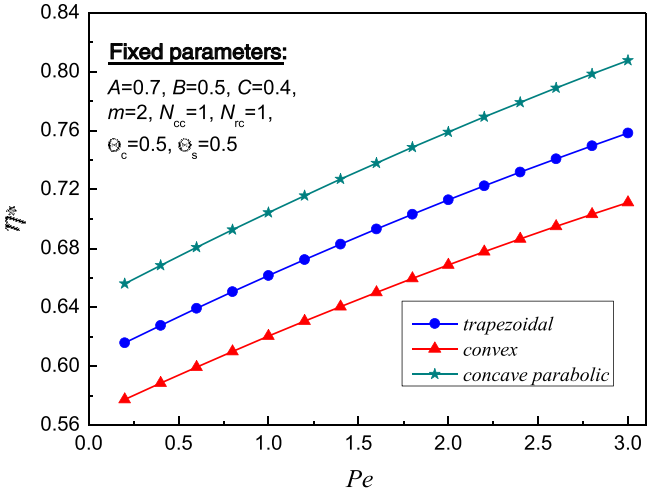

Fig. 15. Effect of Pe on volume adjusted fin efficiency for different cross-sections.

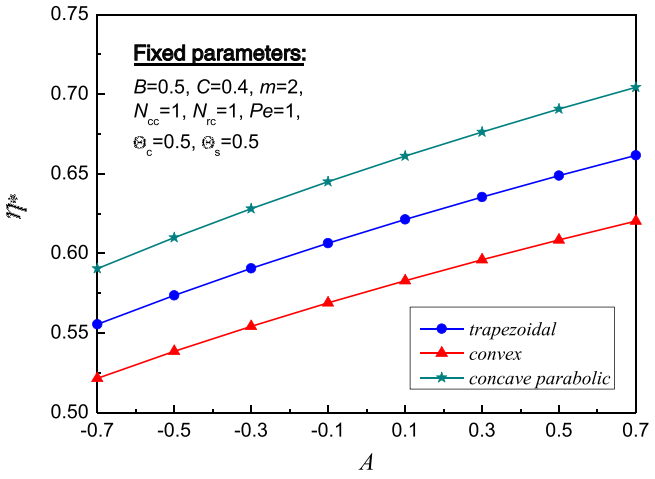

Fig. 16. Effect of A on volume adjusted fin efficiency for different cross-sections.

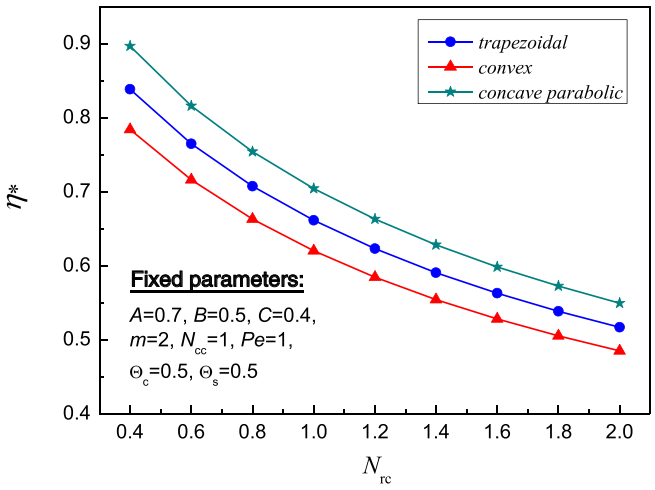

Fig. 18. Effect of N_{rc} on volume adjusted fin efficiency for different cross-sections.

temperature becomes higher, and results in an increase in the fin efficiency. Compared with the efficiencies of trapezoidal and concave parabolic fins, the efficiency of the convex fin is higher. However, this comparison is improper, because it does not take into account the difference in the amount of material for these fins. As shown in Fig. 1, for the same thickness and length, the convex fin consumes more material than the trapezoidal and concave parabolic fins. The volume adjusted fin efficiency is obtained by Eq. (15). Effects of the Peclet number, the thermal conductivity parameter and convective–conductive parameter on the volume adjusted fin efficiency are shown in Figs. 15–18, respectively. In Figs. 15–18, the volume adjusted fin efficiencies of trapezoidal and concave parabolic fins are higher than those of the convex fin.

As shown in Fig. 16, the increasing of thermal conductivity parameter can increase the volume adjusted fin efficiency. The increasing of coefficient of thermal conductivity can enhance conduction heat transfer and increase the dimensionless temperature, and consequently the volume adjusted fin efficiency increases.

Figs. 17 and 18 show effects of convective–conductive parameter and radiative–conductive parameter on the volume adjusted fin efficiency, respectively. As convective–conductive parameter or radiative–conductive parameter increases, it attributes to more convective or radiative heat loss from the fin surface, and results in a decrease in the fin efficiency. Moreover, compared with the decreasing trend in Fig. 17, this trend in Fig. 18 is more obvious. The reason is clear, radiation heat loss plays more obvious impact on the fin efficiency, and radiation heat loss is proportional to the fourth power of temperature difference between radiation sink temperature and surface temperature.

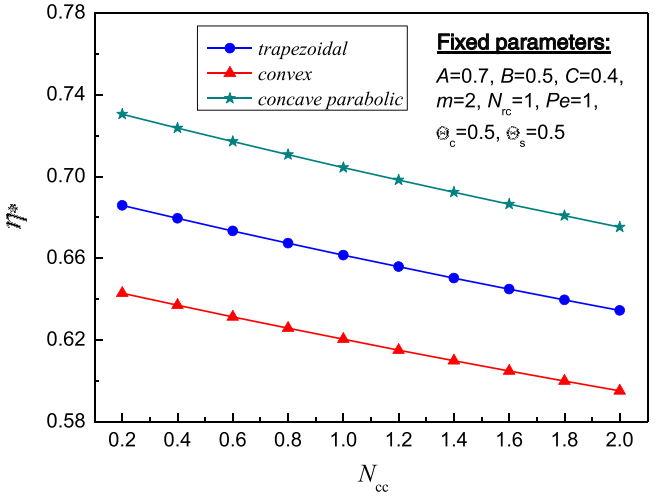

Fig. 17. Effect of N_{cc} on volume adjusted fin efficiency for different cross-sections.

4 . Conclusions

In this paper, SCM is successfully applied to analyze the thermal performances of moving radiative–convective fins of trapezoidal, convex and concave parabolic cross-sections with temperature-dependent thermal conductivity, heat transfer coefficient and surface emissivity. During the solving process, energy equation is expressed as non-dimensional form by dimensionless parameters, the spatial domain of dimensionless temperature is discretized by Lagrange interpolation polynomials, and a particular algorithm is adopted to reduce multiple nonlinearities of energy equation. Effects of physical parameters such as Peclet number, thermal conductivity parameter, emissivity parameter, parameter of heat transfer coefficient, convective–conductive parameter and radiative–conductive parameter on dimensionless temperature, dimensionless fin-tip temperature and fin efficiency are comprehensively investigated. Conclusions can be summarized as follows:

- Compared with available results in references, SCM has a good accuracy for solving heat transfer in the moving fin of complex cross-section with multiple nonlinearities.
- The integral relative error between SCM results and analytical solutions approximately decreases with the exponential trend as the total number of collocation points increases.
- Taking into account the difference in the amount of material for trapezoidal, convex and concave parabolic fins, a volume adjusted fin efficiency is introduced to compare the thermal performances of these fins.

Conflict of interest statement

Authors state that the manuscript does not have any conflict of interest including any financial, personal or other relationships with other people or organizations within three years of beginning the submitted work that could inappropriately influence, or be perceived to influence, the present work.

Acknowledgments

This work was supported by the National Natural Science Foundation of China (Grant Nos. 51206043 and 51210011), and the Specialized

Research Fund for the Doctoral Program of Higher Education (Grant No. 20130036120009).

References

[1] Y.A. Cengel, Heat Transfer: a Practical Approach, second ed. McGraw-Hill Science, London, 2007.
[2] A.D. Kraus, A. Aziz, J.R. Welty, Extended Surface Heat Transfer, Wiley, New York, 2002.
[3] T.L. Bergman, A.S. Lavine, T.P. Incropera, Introduction to Heat Transfer, Wiley, New York, 2011.
[4] A. Aziz, S.M.E. Huq, Perturbation solution for convecting fin with variable thermal conductivity, ASME J. Heat Transf. 97 (1975) 300–301.
[5] S.B. Coskun, M.T. Atay, Fin efficiency analysis of convective straight fins with temperature dependent thermal conductivity using variation iteration method, Appl. Therm. Eng. 28 (2008) 2345–2352.
[6] D.B. Kulkarni, M.M. Joglekar, Residue minimization technique to analyze the efficiency of convective straight fins having temperature-dependent thermal conductivity, Appl. Math. Comput. 215 (2009) 2184–2191.
[7] G. Domairry, M. Fazeli, Homotopy analysis method to determine the fin efficiency of convective straight fins with temperature-dependent thermal conductivity, Commun. Nonlinear Sci. Numer. Simul. 14 (2009) 489–499.
[8] A.A. Sertkaya, S. Bilir, S. Kargicgimath, Experimental investigation of the effects of orientation angle on heat transfer performance of pin-finned surfaces in natural convection, Energy 36 (2011) 1513–1517.
[9] D. Lesnic, P.J. Heggs, A decomposition method for power–law fin-type problems, Int. Commun. Heat Mass Transf. 31 (2004) 673–682.
[10] S. Sadri, M.R. Raveshi, S. Amiri, Efficiency analysis of straight fin with variable heat transfer coefficient and thermal conductivity, J. Mech. Sci. Technol. 26 (2012) 1283–1290.
[11] F. Kahani, M.A. Raji, H.H. Nejad, Analytical solutions and efficiency of the nonlinear fin problem with temperature-dependent thermal conductivity and heat transfer coefficient, Commun. Nonlinear Sci. Numer. Simul. 14 (2009) 3327–3338.
[12] S. Mosayebidorcheh, D.D. Ganji, M. Farzinpoor, Approximate solution of the nonlinear heat transfer equation of a fin with the power–law temperature-dependent thermal conductivity and heat transfer coefficient, Propuls. Power Res. 3 (2014) 41–47.
[13] F. Kani, A. Aziz, Thermal analysis of a longitudinal trapezoidal fin with temperature-dependent thermal conductivity and heat transfer coefficient, Commun. Nonlinear Sci. Numer. Simul. 15 (2010) 590–601.
[14] A. Aziz, M.N. Bouaziz, A least squares method for a longitudinal fin with temperature dependent internal heat generation and thermal conductivity, Energy Convers. Manag. 52 (2011) 2876–2882.
[15] M. Torabi, A. Aziz, Thermal performance and efficiency of convective–radiative T-shaped fins with temperature thermal conductivity, heat transfer coefficient and surface emissivity, Int. Commun. Heat Mass Transf. 30 (2012) 1018–1029.
[16] M. Torabi, Q.B. Zhang, Analytical solution for evaluating the thermal performance and efficiency of convective straight fins with various profiles and considering all non-linearities, Energy Convers. Manag. 66 (2013) 199–201.
[17] M. Torabi, A. Aziz, K.L. Zhang, A comparative study of longitudinal fins of rectangular, trapezoidal and concave parabolic profiles with multiple nonlinearities, Energy 51 (2013) 243–256.
[18] J.S. Hesthaven, E.M. Ronquist, Spectral and High Order Methods for Partial Differential Equations, Springer, Heidelberg, 2010.
[19] D.A. Kopriva, Implementing Spectral Methods for Partial Differential Equations, Springer, Tallahassee, 2009.
[20] J. Shen, T. Tang, L.L. Wang, Spectral Methods: Algorithms, Analysis and Applications, Springer, London, 2011.
[21] A. Karageorghis, T.N. Phillips, Chebyshev spectral collocation methods for laminar flow through a channel contraction, J. Comput. Phys. 84 (1989) 114–133.
[22] B.W. Li, Y.R. Zhao, Y. Yu, Three-dimensional transient Navier–Stokes solvers in cylindrical coordinate system based on a spectral collocation method using explicit treatment of the pressure, Int. J. Numer. Methods Fluids 66 (2011) 284–298.
[23] M. Najafi, K. Hejranfar, V. Esfahanian, Application of a shock-fitted spectral collocation method for computing transient high-speed inviscid flows over a blunt nose, J. Comput. Phys. 257 (2014) 954–980.
[24] F.H. Zeng, H.P. Ma, D. Liang, Energy-conserved splitting spectral methods for two dimensional Maxwell's equations, J. Comput. Appl. Math. 265 (2014) 301–321.
[25] Y. Yu, B.W. Li, A. Thess, The effect of a uniform magnetic field on vortex breakdown in a cylinder with rotating upper lid, Comput. Fluids 88 (2013) 510–523.
[26] X.H. Luo, B.W. Li, J.K. Zhang, Z.M. Hu, Simulation of thermal radiation effects on MHD free convection in a square cavity using Chebyshev collocation spectral method, Numer. Heat Tran. Part A 66 (2014) 1–24.
[27] S. Abbasbandy, T. Hayat, H.R. Ghehsareh, A. Alsaedi, MHD Falkner–Skan flow of Maxwell fluid by rational Chebyshev collocation method, Appl. Math. Mech. 34 (2013) 921–930.
[28] B.W. Li, Y.S. Sun, Y. Yu, Iterative and direct Chebyshev collocation spectral methods for one-dimensional radiative heat transfer, Int. J. Heat Mass Transf. 51 (2008) 5887–5894.
[29] Y.S. Sun, B.W. Li, Spectral collocation method for transient conduction–radiation heat transfer, J. Thermophys. Heat Transf. 24 (2010) 823–832.